Proceedings of the 25th National and 3rd International ISHMT-ASTFE Heat and Mass Transfer Conference (IHMTC-2019), December 28-31, 2019, IIT Roorkee, Roorkee, India.

IHMTC2019-ENE-170

Modelling of Open Thermochemical Energy Storage System for Space Heating using Reduced Order Model

Ankit Mukherjee[a], Rudrodip Majumdar[b], Sandip K. Saha[c,*], Chandramouli Subramaniam[d], Lalit Kumar[a]

[a] Department of Energy Science and Engineering, IIT Bombay
[b] EEP, School of Natural Sciences and Engineering, National Institute of Advanced Studies, IISc campus
[c] Department of Mechanical Engineering, IIT Bombay
[d] Department of Chemistry, IIT Bombay
*Corresponding author email: sandip.saha@iitb.ac.in

ABSTRACT

Thermochemical energy storage (TCES) systems are excellent alternatives for seasonal heat storage due to their high energy densities. In the present work, an open TCES system employed for space heating application based on strontium bromide-water vapour reactive pair is considered. A simplified one-dimensional numerical model of the reactive bed is developed and validated. Further, the effect of variation of the energy density of the reactive bed on the performance of the system is investigated. The global reaction advancement rate is observed to decrease substantially with the increase in the energy density of the reactive bed, for both hydration and dehydration processes. The ratio of the energy storage/extraction rate to the power consumed to blow the moist air through the reactive bed, during both hydration and dehydration processes, is found to decrease with an increasing energy density of the reactive bed.

Keywords: Open Thermochemical Energy Storage, Seasonal Storage, Reduced Order Model.

INTRODUCTION

Thermochemical energy storage (TCES) systems store heat in the form of chemical energy. As compared to other thermal energy storage systems, the energy storage density of these systems is quite high (0.7-1.8 GJ.m^{-3}) [1]. Since the heat is stored in the form of chemical energy, the energy loss to the surroundings is negligible. Thus, TCES systems can be used for seasonal storage of energy for space heating. The system may be charged during the summers when the solar radiation is available in abundance, and the stored energy can be recovered during the winters to maintain thermal comfort conditions in residential spaces. The TCES systems employ reversible endothermic/exothermic solid-gas reactions to store/release energy, such as the reaction of strontium bromide with water vapour: $SrBr_2.6H_2O(s) + \Delta H \rightleftharpoons SrBr_2.H_2O(s) + 5H_2O(g)$. TCES systems can be categorized into closed systems and open systems. Closed systems store the gaseous reactant in a separate vessel to be used as per requirement. In the case of an open system, the atmospheric air is used to carry out the reaction. Open systems are less complex in terms of their design and maintenance. In the present study, open TCES system based on strontium bromide-water vapour reactive pair is selected for further analysis.

Several studies on open TCES system, both numerical and experimental, have been carried out. Michel et al. [2] developed a two-dimensional model for open TCES system based on strontium bromide-water vapour reactive pair and identified mass transfer as the limiting phenomena in open TCES systems. A large scale prototype of the open TCES system based on strontium bromide-water vapour reactive pair was constructed by Michel et al. [3], with an energy density of 0.73 GJ.m^{-3}. Recently, Mukherjee et al. [4] studied the effects of variation of different operating parameters on the performance of open TCES system based on strontium bromide-water vapour reactive pair using a two-dimensional model of the reactive bed.

Review of the previously published literature indicates the need for a simplified and computationally economical, yet reasonably accurate numerical model of the TCES reactor. In the present work, a reduced order model of the reactive bed is developed. Strontium bromide-water vapour reactive pair is selected for the study. The model is validated with the results of previous numerical and experimental studies available in the literature. The model is then used to investigate the effect of variation of reactive bed energy

density on the performance of the system, during both the hydration and dehydration processes.

MATHEMATICAL MODELING

A reactive bed of strontium bromide salt is considered as shown in figure 1. The dimensions of the reactive bed are taken from the literature [2]. The top surface of the reactive bed serves as the inlet for moist air flow, which flows out of the reactive bed from its bottom surface. The bottom surface of the bed is exposed to atmospheric pressure. The four surfaces at the sides of the reactive bed are considered thermally insulated and impermeable to the gases. During hydration, the ambient air containing water vapour (reactant) is sent to the reactive bed. During dehydration, the ambient air is heated prior to sending to the reactive bed to supply the heat required for the endothermic reaction. The flow rate of moist air is maintained constant during both the hydration and dehydration processes.

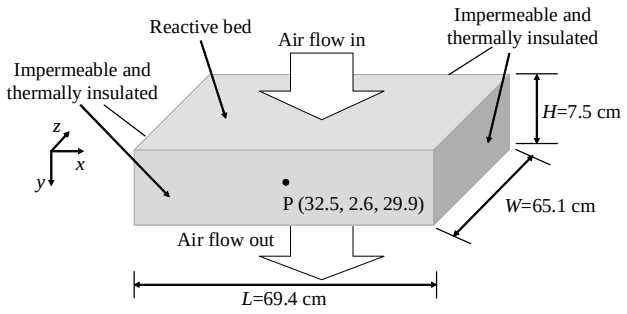

Figure 1: Schematic diagram of the reactive bed

The reactive bed is modelled as a pseudo-homogeneous porous domain. A one-dimensional simplified model of the reactive bed is developed. The reactive salt, the water vapour, and the dry air in the reactive bed are assumed to exist in local thermal equilibrium with each other. This assumption is valid for the present study as the size of the pores present in the reactive bed are very small, and the variation in the thermal properties of the bed is not significantly large [5]. Other assumptions taken into consideration are: (i) the moist air is a homogeneous mixture of dry air and water vapour, and follows ideal gas behaviour, (ii) the properties of the reactive bed are invariant with temperature, (iii) the flow rate of moist air is constant and uniform throughout the reactive bed and follows the Darcy law, (iv) heat transfer in the reactive bed is due to conduction and convection. Radiation heat transfer is not considered as the temperatures in the reactive bed are low [6].

Governing equations:

(a) Darcy law [2]:

$$\boldsymbol{u} = -\frac{\kappa_b}{\mu_a}\frac{\partial P}{\partial y} \tag{1}$$

where $\boldsymbol{u}$ is Darcy velocity, P is the pressure, κ_b is the permeability of the reactive bed, and μ_a is the dynamic viscosity of air.

(b) Reaction kinetics [5]:

$$\frac{\partial \alpha}{\partial t} = k_r(1-\alpha)^p \alpha^q \left(\frac{P_w - P_w^*(T)}{P_w}\right) \tag{2}$$

where α is local reaction advancement, $k_r = k_0 exp\left(\frac{-E_{ac}}{RT}\right)$ is kinetic factor, k_0 is pre-exponential factor, E_{ac} is the activation energy, P_w is the local partial pressure of water vapour, and P_w^* is equilibrium water vapour pressure defined in equation (6), p = 1 and q = 0 during hydration, and p = 0 and q = 1 during dehydration.

(c) Moist air molar balance [2]:

$$\frac{\partial(\phi_b n_m)}{\partial t} + \frac{\partial}{\partial y}(n_m \boldsymbol{u}) + \psi n_b \frac{\partial \alpha}{\partial t} = 0 \tag{3}$$

where ϕ_b is the bed porosity, n_m is the moist air molar concentration, n_b is the reactive bed molar density, and ψ is the stoichiometric coefficient.

(d) Water vapour molar balance [2]:

$$\phi_b n_m \frac{\partial(\xi_w)}{\partial t} - \frac{\partial}{\partial y}\left(n_m D_{wa}\frac{\partial \xi_w}{\partial y}\right) + (1-\xi_w)\psi n_b \frac{\partial \alpha}{\partial t} + n_m \boldsymbol{u}\frac{\partial \xi_w}{\partial y} = 0 \tag{4}$$

where ξ_w is the water vapour mole fraction in moist air, D_{wa} is the binary diffusion constant for air-water vapour mixture.

(e) Energy balance [2]

$$(\phi_b n_m c_m + n_b c_b)\frac{\partial T}{\partial t} - \frac{\partial}{\partial y}\left(\lambda_b \frac{\partial T}{\partial y}\right) + n_m c_m \boldsymbol{u}\frac{\partial T}{\partial y} - \Delta H n_b \frac{\partial \alpha}{\partial t} = 0 \tag{5}$$

where c_m and c_b are the specific heats of moist air and reactive bed, respectively, and λ_b is the effective thermal conductivity of reactive bed which is assumed constant throughout the process.

The equilibrium water vapour pressure P_w^* in equation (2) is given by the Clausius-Clapeyron equation defined as [2],

$$P_w^* = 10^5 \cdot exp\left(\frac{-\Delta H}{\psi RT} + \frac{\Delta S}{\psi R}\right) \tag{6}$$

where ΔH and ΔS are the enthalpy and entropy of the reaction, respectively.

The porosity of the reactive bed and the specific heat of the reactive bed and that of moist air are assumed to vary linearly with the local reaction advancement as [2],

$$\phi_b = (1-\alpha)\phi_d + \alpha\phi_h \tag{7}$$

$$c_m = (1-\xi_w)c_a + \xi_w c_w \tag{8}$$

$$c_b = (1-\alpha)c_d + \alpha c_h \tag{9}$$

where ϕ_d, ϕ_h are the porosities of dehydrated and hydrated reactive bed, respectively, c_a, c_w are the specific heats of dry

air and water vapour, respectively, and c_d, c_h are the specific heats of dehydrated and hydrated reactive salt, respectively.

Reactive bed permeability (κ_b) is a function of local reaction advancement, and is evaluated as [2],

During hydration: $$\kappa_b = \frac{1}{\frac{(1-\alpha)}{\kappa_d}+\frac{\alpha}{\kappa_h}} \quad (10)$$

During dehydration: $$\kappa_b = (1-\alpha)\kappa_d + \alpha\kappa_h \quad (11)$$

where κ_d and κ_h are the permeabilities of dehydrated and hydrated reactive bed, respectively.

The binary diffusion coefficient in equation (4) is assumed constant and is evaluated at temperature T = 298 K and pressure P = 1 atm by using the following expression [7],

$$D_{wa} = 1.758 \times 10^{-4} \frac{T^{1.685}}{P} \quad (12)$$

Global reaction advancement is evaluated by averaging the local reaction advancement over the volume of the reactive bed (V_b) as,

$$\alpha_{glo} = \frac{1}{V_b}\int_{V_b} \alpha \, dV_b \quad (13)$$

Initial and boundary conditions:

During hydration: $$\alpha(y, t = 0) = 0 \quad (14)$$

During dehydration: $$\alpha(y, t = 0) = 1 \quad (15)$$

For both the hydration and dehydration processes, the following boundary conditions hold:

$$T(y, t = 0) = T_{amb} \quad (16)$$

$$P(y, t = 0) = P_{amb} \quad (17)$$

$$P_w(y, t = 0) = P_w^*(T_{amb}) \quad (18)$$

$$P(y = H) = P_{amb} \quad (19)$$

$$P_w(y = 0, t) = P_{w,in} \quad (20)$$

where T_{amb} is the ambient temperature, P_{amb} is the ambient pressure, $P_w^*(T_{amb})$ is the equilibrium water vapour pressure at ambient temperature obtained by using equation (6), and $P_{w,in}$ is the partial pressure of moist air entering the reactive bed. The change in the temperature of air when entering the reactive bed is expressed as a heat flux condition at the inlet [2],

$$q_{in}^{"} = \phi_b n_m c_m v(T|_{y=0} - T_{amb}) \quad (21)$$

The outflow boundary condition is assumed at the bottom boundary,

$$\frac{\partial T}{\partial y} = 0 \quad (22)$$

The thermophysical properties of the reactive salt ($SrBr_2.6H_2O$) and moist air used for the present numerical study have been taken from published literature [2, 6, 8-9]. The governing equations are discretized using the Power law scheme and fully implicit scheme. The convergence criterion is set as 10^{-8}. The discretized equations are solved using a numerical code written in MATLAB. Grid independence study with uniform grid spacing of 40 (grid 1), 80 (grid 2), and 160 elements (grid 3) is carried out for the dehydration phase, keeping the time-step fixed at 0.005 s. The maximum difference in the temperature at the outlet of the reactive bed between grid 1 and grid 2 is found to be 3.89 K, while the same between grid 2 and grid 3 is found to be 2.23 K. Hence, grid 2 is selected for the present study.

Model validation:

The numerical model is validated with the results of numerical and experimental study available in the literature [3, 4]. The values of different parameters used in the validation study are listed in Table 1. Michel et al. [3] carried out the experimental study on a prototype consisting of eight trays filled with reactive salt stacked parallel with respect to the flow of moist air. The overall flow rate to the prototype is reported as 290 m^3/h, however, the rate of moist air flow to the individual trays are not provided [3]. Therefore, following the assumption of equal flow distribution among the trays as considered in the previous numerical study [4], a constant flow rate value of $\dot{V}$ = 36.25 m^3/h is employed in the present study.

Table 1: Values of parameters employed in validation study

Parameter	Value
k_0 (s^{-1})	5.5×10^5
E_{ac} (J mol^{-1})	55000
n_b(mol m^{-3})	4145.40
$P(t = 0)$ (Pa)	101325
$P_{w,in}$ (Pa)	981
$T(t = 0)$ (K)	298
T_{amb} (K)	298
$\dot{V}$ ($m^3 h^{-1}$)	36.25
ϕ_h (-)	0.38
ϕ_d (-)	0.68
κ_h (m^2)	5.9×10^{-11}
κ_d (m^2)	5.7×10^{-10}
ψ	5

Figure 2 depicts the temporal evolution of the local temperature at point P (Fig. 1) during hydration phase, obtained from the present reduced order model, and the same is compared with the results reported in the literature [3, 4]. The local temperature profile obtained from the reduced order model shows good agreement with the temperature profile obtained from two-dimensional model reported in the literature [4], and agrees well with the trend of the temperature profile obtained by experiments [3]. The discrepancy in the values of local temperature obtained by the reduced order model and those obtained by experiments

could plausibly be due to neglecting the effect of salt agglomeration, and the effect of non-homogeneity of the reactive bed due to the spatial variation of porosity, in the present model. Furthermore, as suggested by Michel et al. [3], the creation of preferential air passages along the thermocouples inserted in the reactive bed in the experimental prototype could also be one of the reasons for the discrepancy mentioned above.

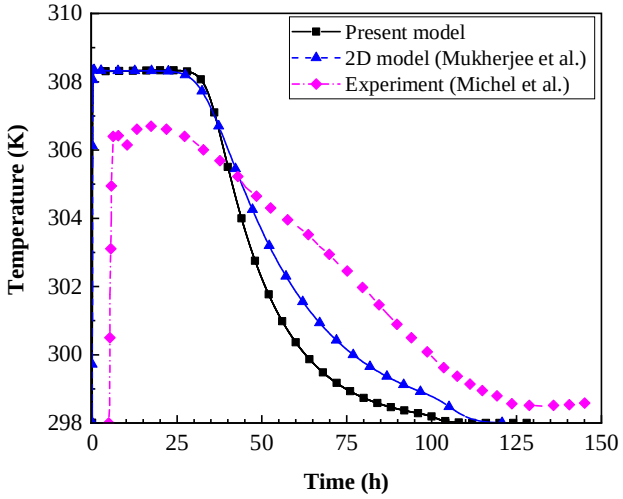

Figure 2: Comparison of the local temperature profile at point P (shown in Fig. 1) during hydration as obtained by the present model with the two-dimensional (2D) numerical model reported by Mukherjee et al. [4] and with experimental data reported by Michel et al. [3]

RESULTS AND DISCUSSION

Effect of reactive bed energy density:

The increase in the reactive salt packing density in the bed enhances the energy density (ω_b) of the reactive bed. Nevertheless, increasing the salt packing density reduces the void spaces (porosity) in the bed. According to the Kozeny-Carman equation (equations (25) and (26)), which relates the porosity of a packed bed with its permeability, the decrease in porosity decreases the permeability of the reactive bed. For a constant air flow through the bed, decreased permeability results in increased pressure drop across the bed (equation (1)), and hence, more energy consumption to operate the system. In order to assess the effect of the energy density of the reactive bed on the performance of TCES system, simulations are run for both the dehydration and hydration phases for three different values of energy density: 1.25, 1.35, and 1.45 GJ/m^3, keeping other parameters fixed. The corresponding values of porosity for the dehydrated and the hydrated salt in the reactive bed for the above mentioned three cases are obtained using the following relations [2]:

$$\phi_d = 1 - \frac{\omega_b M_d}{\Delta H \rho_d} \quad (23)$$

$$\phi_h = 1 - \frac{\omega_b M_h}{\Delta H \rho_h} \quad (24)$$

where M_d and M_h are the molar masses of the reactive salt in dehydrated and hydrated states, respectively, and ρ_d and ρ_h are the true mass densities of the reactive salt in dehydrated and hydrated states, respectively.

In order to evaluate the permeability of the hydrated and dehydrated salt bed for different energy densities, Kozeny-Carman relation is used [1],

$$\kappa_d = \frac{\phi_d^3 d_p^2}{180(1-\phi_d)^2} \quad (25)$$

$$\kappa_h = \frac{\phi_h^3 d_p^2}{180(1-\phi_h)^2} \quad (26)$$

where κ_d and κ_h are the permeabilities of dehydrated and hydrated reactive bed, respectively, and d_p is the diameter of salt grain.

The diameter of the salt grain (d_p) in equations (25) and (26) is assumed to remain unchanged with the progress of the reaction and with the change in the energy density of the bed, and is calculated using the values of permeability and porosity of the dehydrated salt bed from the literature [2, 4]. Table 2 lists the values of porosity and permeability for the three cases of energy densities considered in this study. Values of other parameters used in the numerical study are listed in Table 3.

Table 2: Porosity and permeability values for different energy densities of reactive bed

ω_b (GJ/m^3)	ϕ_d	ϕ_h	κ_d (m^2)	κ_h (m^2)
1.25	0.72	0.45	1.90×10^{-9}	12.22×10^{-11}
1.35	0.69	0.40	1.48×10^{-9}	7.68×10^{-11}
1.45	0.67	0.36	1.17×10^{-9}	4.70×10^{-11}

Table 3: Values of parameters employed in the numerical study

Parameter	Value (hydration)	Value (dehydration)
k_0 (s^{-1})	5.5×10^5	5.5×10^5
E_{ac} (J mol^{-1})	55000	55000
$P(t=0)$ (Pa)	101325	101325
$P_{w,in}$ (Pa)	981	1500
$T(t=0)$ (K)	298	303
T_{in} (K)	298	353
$\dot{V}$ (m^3 h^{-1})	40	40

To evaluate the performance of the TCES system during the hydration and dehydration processes, few performance parameters are defined. In order to compare the energy storage/extraction rate with the power expended by the moist air flow in overcoming the frictional losses in the reactive bed, the parameter ζ is adopted [10], that is defined as the ratio of the energy storage/extraction rate to the power consumed to blow the moist air through the reactive bed

during both the hydration and dehydration processes. This is expressed mathematically as,

$$\zeta = \frac{E_{ext} \text{ or } E_{sto}}{E_P} \quad (27)$$

where E_{ext} is the rate of extraction of energy from the reactive bed during the hydration process, E_{sto} is the rate of storage of energy in the reactive bed during the dehydration process, and E_P is the power consumed in blowing the moist air through the reactive bed.

The rate of energy extraction (E_{ext}) during the hydration process is given by,

$$E_{ext} = \Delta H n_b V_b \frac{d\alpha_{glo}}{dt} \quad (28)$$

The rate of energy stored during the dehydration process is evaluated as,

$$E_{sto} = -\Delta H n_b V_b \frac{d\alpha_{glo}}{dt} \quad (29)$$

The negative sign in equation (29) is used to make E_{sto} positive, since $\frac{d\alpha_{glo}}{dt}$ is negative during the dehydration process.

Assuming the flow of moist air through the reactive bed to be incompressible, E_P is evaluated as,

$$E_P = \dot{V} \Delta P \quad (30)$$

where ΔP is the pressure drop across the reactive bed.

The global conversion X for the hydration and dehydration process is defined as,

$$X = \alpha_{glo} \quad \text{(during hydration)} \quad (31)$$

$$X = (1 - \alpha_{glo}) \text{ (during dehydration)} \quad (32)$$

Figure 3 depicts the temporal variations of the temperature of air leaving the reactive bed and the global reaction advancement during the hydration process for different energy densities of the reactive bed. The outlet temperature for the three different ω_b values are observed to increase to ~307.6 K and then remain almost constant for a substantial period of time forming a plateau, before decreasing to the temperature level of the incoming air. The plateau temperatures for the three cases of ω_b are almost equal, with the maximum difference being 0.027 K. The length of the temperature plateau is, however, greater for a higher value of ω_b. Due to the higher density of the reactive bed for higher ω_b, the amount of water vapour required to maintain the same reaction advancement rate for higher ω_b is required to be higher. However, the air flow rate and the inlet partial water vapour pressure are fixed for all the cases of ω_b, thereby fixing the rate of transport of water vapour to the reactive bed. Therefore, the reaction advancement rate for higher ω_b is slower, as evident from the lengthier temperature plateaus and the global reaction advancement profiles shown in figure 3. The average rate of global reaction advancement is found to decrease by 10.78% with the increase in ω_b from 1.25 to 1.45 GJ.m^{-3}.

Figure 4 illustrates the temporal variations of outlet temperature of air and the global reaction advancement during the dehydration process for different energy densities of the reactive bed. The outlet temperatures are observed to rise to ~327.5 K, after that remain constant before rising to the temperature level of the incoming air. The maximum difference between the plateau temperatures for the three cases of ω_b is found to be 0.012 K, which is very small. Similar to the hydration process, the temperature plateaus are observed to be lengthier for higher ω_b. The increase in ω_b results in increased heat capacity of the reactive bed. Consequently, the rate of rise of temperature of the reactive bed decreases with increasing ω_b, effectively decreasing the rate of increase of equilibrium water vapour pressure P_w^*, thereby resulting in decreased global reaction advancement rate (figure 4). The average rate of global reaction advancement is found to decrease by 14.39% with an increase in ω_b by 200 MJ.m^{-3}.

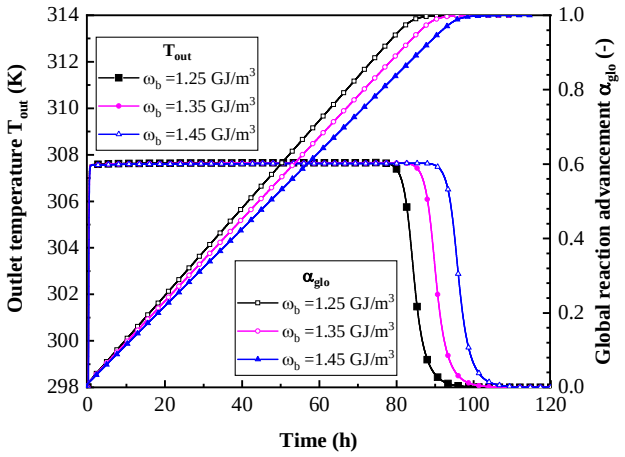

Figure 3: Temporal profiles of outlet temperature and global reaction advancement during hydration for three different values of reactive bed energy densities

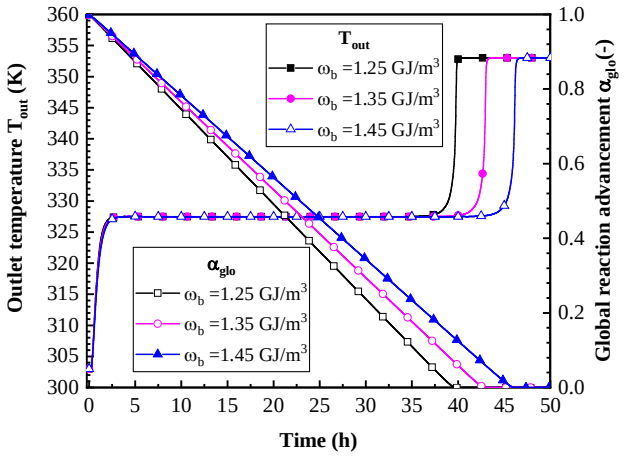

Figure 4: Temporal profiles of outlet temperature and global reaction advancement during dehydration for three different values of reactive bed energy densities

Figure 5 shows the variation of ζ with global conversion (X) for different values of ω_b. In the case of hydration, the profiles show a decreasing trend for ζ for all the values of ω_b due to the decrease in the permeability of the reactive bed with the progress of hydration (equation 10). Nevertheless, with the increase in ω_b, ζ is observed to decrease. This is due to the combined effect of slower reaction advancement rate and higher pressure drop across the reactive bed for higher ω_b. During dehydration, the profiles of ζ are observed to increase with X, and reach a maximum value near the end of the dehydration, and then diminish. The increasing trend of ζ can be attributed to the decrease in the pressure drop across the reactive bed with the progress of dehydration. With an increase in ω_b, the values of ζ are observed to decrease due to lower reaction advancement rate and higher pressure drop.

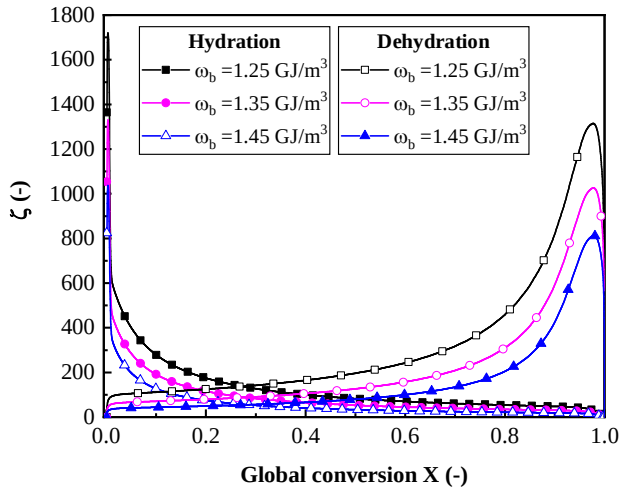

Figure 5: Variation of ζ with global reaction advancement during hydration and dehydration for three different values of reactive bed energy densities

CONCLUSIONS

In the present work, a simplified one-dimensional reduced order model of the reactive bed in an open TCES system is developed. The model is validated with the results of the numerical study and the experimental data available in the literature. The model is then used to assess the performance of the TCES system for different energy densities of the reactive bed during the hydration and the dehydration processes. The increase in the energy density of the reactive bed has a negligible effect on the plateau temperature of the air at the outlet of the reactive bed, for both the hydration and the dehydration processes. The average rate of global reaction advancement is found to decrease by 10.78% during the hydration process, and by 14.39% during the dehydration process, for an increase in energy density by 200 MJ.m^{-3}. The parameter ζ, which is the ratio of the rate of energy stored/extracted to the power expended in blowing the moist air through the reactive bed, is found to decrease with the increase in the energy density of the reactive bed, for both the hydration and dehydration processes. It may be concluded that with the increase in the energy density of the reactive bed, the system becomes more compact; however, the power expended in hydrating/dehydrating the reactive bed also increases significantly. The reduced order model developed in the present study can be further used to study the effects of various design and operating parameters on the performance of the open TCES system.

References

1. Michel, B., N. Mazet, S. Mauran, D. Stitou, and J. Xu. 2012. “Characterization and modeling of a high density reactive bed.” *Energy* 47:553-63. doi:10.1016/j.energy.2012.09.029.
2. Michel, B., P. Neveu, and N. Mazet. 2014. “Comparison of closed and open thermochemical processes, for long-term thermal energy storage applications.” *Energy* 72:702-16. doi:10.1016/j.energy.2014.05.097.
3. Michel, B., N. Mazet, and P. Neveu. 2016. “Experimental investigation of an open thermochemical process operating with a hydrate salt for thermal storage of solar energy: Local reactive bed evolution.” *Applied Energy* 180:234-44. doi:10.1016/j.apenergy.2016.07.108.
4. Mukherjee, A., R. Majumdar, S.K. Saha, L. Kumar, and C. Subramaniam. 2019. “Assessment of open thermochemical energy storage system performance for low temperature heating applications.” *Applied Thermal Engineering* 156: 453-70. doi:10.1016/j.applthermaleng.2019.04.096.
5. Lele, A.F. 2015. “Thermochemical Heat Storage System for Households: Thermal Transfers Coupled to Chemical Reaction Investigations.” doi:10.1007/978-3-319-41228-3.
6. Olives, R., and S. Mauran. 2001. “A highly conductive porous medium for solid-gas reactions: Effect of the dispersed phase on the thermal tortuosity.” *Transport in Porous Media* 43:377-94. doi:10.1023/A:1010780623891.
7. Liu, H., and K. Nagano. 2014. “Numerical simulation of an open sorption thermal energy storage system using composite sorbents built into a honeycomb structure.” *International Journal of Heat and Mass Transfer* 78:648-61. doi:10.1016/j.ijheatmasstransfer.2014.07.034.
8. Hilsenrath, J., C.W. Beckett, W.S. Benedict, and L. Fano. 1955. “Tables of Thermal Properties of Gases: Comprising Tables of Thermodynamic and Transport Properties of Air, Argon, Carbon Dioxide, Carbon Monoxide, Hydrogen, Nitrogen, Oxygen and Steam.” United States Department of Commerce.
9. Wagner, W., and H-J. Kretzschmar. 2008. “International steam tables - properties of water and steam based on the industrial formulation IAPWS-IF97.” Springer-Verlag Berlin Heidelberg.
10. Malley-Ernewein, A., and S. Lorente. 2019. “Constructal design of thermochemical energy storage.” *International Journal of Heat and Mass Transfer* 130:1299-306. doi:10.1016/j.ijheatmasstransfer.2018.10.097.